Mechanism of Anti-Inflammatory Activity of TLR4-Interacting SPA4 Peptide

Shanjana Awasthi[*], **Gaurav Kumar**[*,1], **Vijay Ramani**[*,2], **Vibhudutta Awasthi**[†], **Karla K. Rodgers**[‡], **Jun Xie**[*,1], **Jacob Beierle**[*,3], **Gertrude Kyere-Davies**[*], **Bhupinder Singh**[*], **Negar Rahman**[*], **Asif Alam Chowdhury**[*], **Neha Chataut**[*]

[*]Department of Pharmaceutical Sciences, College of Pharmacy, University of Oklahoma Health Sciences Center, Oklahoma City, OK

[†]Research Imaging Facility, College of Pharmacy, University of Oklahoma Health Sciences Center, Oklahoma City, OK

[‡]Department of Biochemistry and Molecular Biology, College of Medicine, University of Oklahoma Health Sciences Center, Oklahoma City, OK

Abstract

The TLR4-interacting SPA4 peptide suppresses inflammation. We assessed the structural and physicochemical properties and binding of SPA4 peptide to TLR4–MD2. We also studied the changes at the whole transcriptome level, cell morphology, viability, secreted cytokines and chemokines, and cell influx in cell systems and mouse models challenged with LPS and treated with SPA4 peptide. Our results demonstrated that the SPA4 peptide did not alter the cell viability and size and only moderately affected the transcriptome of the cells. Computational docking and rendering suggested that the SPA4 peptide intercalates with LPS-induced TLR4–MD2 complex. Results with alanine mutations of D-2 amino acid and NYTXXXRG-12–19 motif of SPA4 peptide suggested their role in binding to TLR4 and in reducing the cytokine response against LPS stimulus. Furthermore, therapeutically administered SPA4 peptide significantly suppressed the secreted levels of cytokines and chemokines in cells and bronchoalveolar lavage fluids of

Address correspondence and reprint requests to: Dr. Shanjana Awasthi, Department of Pharmaceutical Sciences, College of Pharmacy, University of Oklahoma Health Sciences Center, 1110 N. Stonewall Avenue, Oklahoma City, OK 73117. Shanjana-Awasthi@ouhsc.edu.
[1]Current address: Oklahoma Medical Research Foundation, Oklahoma City, OK.
[2]Current address: University of Texas Southwestern Medical Center, Dallas, TX.
[3]Current address: Boston University, Boston, MA.

LPS-challenged mice. The results suggest that the SPA4 peptide intercalates with LPS-induced TLR4 complex and signaling for the suppression of inflammation.

INTRODUCTION

Acute lung injury (ALI) induced by infectious or inflammatory stimuli leads to the more severe condition of acute respiratory distress syndrome (ARDS) and remains a major cause of mortality and morbidity. An increased accumulation of inflammatory mediators and pathogen- and damage-associated molecular patterns in lung and systemic circulation are considered hallmarks of ALI and ARDS (1). In the United States, ARDS-associated mortality is ~40% (2). Most often, patients are admitted to intensive care units and are provided life-supportive therapy, mechanical ventilation, and treatment with antimicrobial agents. Currently, there is no effective therapy available for the treatment of ALI or ARDS (3). As the outcomes of ongoing clinical trials with low-dose hydrocortisone, dexamethasone, vitamin C, vitamin D, GM-CSF, nebulized heparin, aspirin, and allogeneic mesenchymal stem cells (reviewed in Refs. 3 and 4) become available, novel therapies are being designed and evaluated to help reduce the inflammation and tissue injury and improve the clinical condition of patients with ALI and ARDS.

Gram-negative bacterial LPS or endotoxin can cause airway inflammation, compromised lung function, and airway hyperreactivity (5, 6). An ambient level of endotoxin is associated with asthma exacerbation in children with asthma (7, 8). Even when bacteria are killed as a result of antibiotic treatment, an elevated level of LPS can cause severe lung inflammation, eventually leading to ALI and ARDS. Intratracheal administration of LPS induces lung inflammation and tissue damage in different animal models (9–11) and closely mimics the clinical condition of such patients (12). LPS is primarily recognized by TLR4. The activation of TLR4 induces a complex network of cellular signaling, resulting in the release of a variety of inflammatory mediators, including cytokines, chemokines, and stress ligands. The accumulation of inflammatory mediators eventually contributes to tissue injuries and edema. LPS binding to TLR4 and activation of cell signaling involve multiple steps. The LPS conjugates with LPS-binding protein (LBP) and is transferred to CD14, myeloid differentiation protein 2 (MD2), and TLR4 in a stepwise manner. The LBP, CD14, and MD2 do not possess cytoplasmic domains. The LPS-stimulated dimerization of transmembrane TLR4 in complex with MD2 proteins forms a large M-shaped structure responsible for inducing intracellular inflammatory signaling (13). The dimer of LPS–MD2–TLR4 conjugates with intracellular adaptor proteins through the cytoplasmic domain of TLR4 and induces NF-κB and activator protein-1 (AP-1) transcription factors, leading to the release of inflammatory mediators and physiological outcomes.

In our previously published report, we demonstrated that the purified lung surfactant protein-A (SP-A) interacts with TLR4, and suppresses the inflammatory cytokine response, yet maintains bacterial phagocytosis (14, 15). These findings led us to examine whether short TLR4-interacting regions of SP-A can maintain some of the host defense functions of SP-A. Using computational molecular modeling and docking and peptide screening approaches, we identified TLR4-interacting regions of SP-A (15). Our work revealed that the lead SPA4

peptide (amino acids: GDFRYSDGTPVNYTNWYRGE) binds to recombinant extracellular TLR4 protein in complex with MD2. Furthermore, the SPA4 peptide suppresses the TLR4–MyD88-induced inflammatory response against LPS (a potent ligand of TLR4) (15–17). Our results also showed that the SPA4 peptide treatment reduces LPS–TLR4–NF-κB signaling and priming of the NLRP3 inflammasome by ATP, an endogenous stress ligand and NLRP3 inducer (18).

In this work, we have investigated the mechanism of action of SPA4 peptide at the subunit level in cell systems and in a mouse model of LPS-induced lung inflammation. Our results demonstrate that the D-2 amino acid and NYTXXXRG-12–19 motif on either side of the U-shaped structure of SPA4 peptide are critical for interaction with the TLR4–MD2 complex and in reducing the cytokine response against LPS stimulus. There was no significant change in cell viability and size of SPA4 peptide–treated cells. The gene expression profiles of LPS-challenged and SPA4 peptide–treated cells (L + S groups) and cells treated with SPA4 peptide alone were moderately affected as compared with LPS-challenged cells (L group) and vehicle-treated cells, respectively. However, the secreted levels of inflammatory cytokines and chemokines were significantly reduced in L + S groups. Correspondingly, intratracheally administered SPA4 peptide reduced the inflammatory response in LPS-challenged mice.

MATERIALS AND METHODS

Animals

Five- to six-week-old female C57BL6 mice were purchased from The Jackson Laboratory (Bar Harbor, ME) and were housed for at least 1 wk for acclimatization before the start of experiments. We included age-matched female mice in two separate experiments performed on different occasions. Up to five mice in a group were housed together. The animal studies were approved by the Institutional Animal Care and Use and Biosafety Committees at the University of Oklahoma Health Sciences Center (OUHSC), Oklahoma City, OK.

SPA4 peptide and alanine mutants

SPA4 peptide (amino acids: GDFRYSDGTPVNYTNWYRGE), hydrazinonicotinamide (HYNIC) linker–conjugated SPA4 peptide, and alanine mutants of SPA4 peptide D-2→A [amino acids: G(A)FRYSDGTPVNYTNWYRGE] and NYTXXXRG-12–19→AAAXXXAA [amino acids: GDFRYSDGTPV(AAA)NWY(AA)E] were synthesized at GenScript (Piscataway, NJ). The purity of each batch of the peptide was confirmed by mass spectroscopy and HPLC. The stock solutions of peptides were prepared in endotoxin-free water.

Physicochemical characteristics of SPA4 peptide and mutants

We assessed the structural features of SPA4 peptide and mutants by circular dichroism (CD) spectroscopy. The SPA4 peptides and mutant peptides were diluted to 200 μg/ml in 75% methanol before CD spectroscopy, as described earlier (19). The CD signal was recorded in millidegrees. The CD spectra were obtained at a temperature of 20°C, with a 0.1-cm cuvette pathlength and three accumulations per spectrum. The SPA4 peptide

and mutants diluted to 2 mg/ml in endotoxin-free water were subjected to UV-visible (UV-VIS) spectrophotometry at the wavelength range 200–700 nm on a BioTek reader (BioTek, Winooski, VT). In addition, predictions on physicochemical properties (such as hydrophobicity, hydrophobic moment, aliphatic index, isoelectric point, Boman index, charge, and stability) were obtained using established programs and were compared for SPA4 peptide and alanine mutants (20–24).

In silico analysis of SPA4 peptide and a computationally docked model of SPA4 peptide in association with the extracellular TLR4–MD2 complex

The top-ranked nuclear magnetic resonance (NMR) structure of SPA4 peptide was visually rendered and was analyzed for electrostatic potential using the Adaptive Poisson-Boltzmann Solver plug-in within the PyMOL (Schrödinger) program (25). The NMR structure of SPA4 peptide was solved and published earlier (19). The SPA4 peptide structure was further analyzed after creating an alanine mutation of D-2 residue and NYTXXXRG-12–19 motif with PyMOL.

Subsequently, the NMR structure of SPA4 peptide was docked onto the available structure of the extracellular TLR4–MD2 complex (Protein Data Bank [PDB] identifier: 3FXI) using the GRAMM-X Protein-Protein Docking Web Server (University of Kansas) (26). In silico rendering of the structures of SPA4 peptide and SPA4 peptide–extracellular TLR4–MD2 complex was performed using the Chimera (University of California, San Francisco), PyMOL, and Visual Molecular Dynamics (University of Illinois at Urbana-Champaign) programs. The D-2 residue and NYTXXXRG-12–19 motif of SPA4 peptide were mutated within the top-ranked NMR structure of SPA4 peptide and computationally docked model of the SPA4 peptide–extracellular TLR4–MD2 complex. The protein–protein interfaces were identified based on atoms around 5-Å distance from the SPA4 peptide and its alanine mutants. Interactions, contacts, clashes, and surfaces were studied.

Cell culture and maintenance

Human embryonic kidney epithelial (HEK)293 cells and mouse bone marrow-derived JAWS II dendritic cells (both obtained from American Type Culture Collection, Manassas, VA) were maintained as described earlier (17). Primary mouse alveolar macrophages were harvested per our previously published report (18). The morphology and viability of the cells were determined by Diff-Quik staining, light microscopy, and the conventional trypan blue dye exclusion method, respectively.

Cell viability

The effect of SPA4 peptide on cell viability was determined by MTT assay (27). In brief, the JAWS II cells (100,000 cells per well) were treated with SPA4 peptide (10 and 75 μM) and were incubated for 45 min or 2 h at 37°C with 5% CO_2. The MTT solution (20 μl of 5 mg/ml stock solution in PBS; Alfa Aesar, Haverhill, MA) was added. The cells were incubated for 2 h at 37°C with 5% CO_2 and lysed with 100 μl of lysis buffer (10% NaDodSO$_4$, SDS, and 45% dimethylformamide solution adjusted to pH 4.5 with glacial acetic acid). The absorbance was read at 570 nm on a spectrophotometer (BioTek). JAWS II

cells heated at 75°C for 10 min (90% dead cells as determined by trypan blue staining) were included as controls.

We also determined the viability of HEK293 cells by trypan blue staining. One million cells per well were treated with SPA4 peptide (10 and 75 μM) and were incubated for 45 min and 2, 4, and 24 h at 37°C with 5% CO_2. The cells were scraped and stained with trypan blue solution (Thermo Fisher Scientific, Waltham, MA). The cells were then counted using a hematocytometer. Percentage of viability was calculated by the ratio of trypan blue–negatively stained cells to the total cells. Photomicrographs were collected with 40× objective lens and subjected to measurement of cell diameter using the National Institutes of Health ImageJ program.

Binding of SPA4 peptide to TLR4 at the cellular level

Mammalian two-hybrid assay.—To study the interaction between SPA4 peptide and TLR4, HEK293 cells were included in the assay (17). About 50,000 HEK293 cells were cotransfected with pACT-SPA4, pBIND-TLR4, and pG5Luc plasmid DNAs using 0.2 μg of each plasmid DNA and 1 μl of Lipofectamine 2000 reagent, as described previously (17). After 24 h of transfection, the cells were lysed in lysis buffer provided with the dual luciferase assay kit (Promega, Madison, WI). Luminescence activity associated with Renilla and Firefly luciferase was quantified simultaneously (BioTek). The pACT-SPA4 and pBIND-TLR4 plasmid DNAs encode SPA4 peptide and full-length human TLR4, respectively. Firefly luciferase–associated luminescence was recorded as an indicator of the interaction of SPA4 peptide with TLR4. Renilla luciferase–associated luminescence provided an internal control for transfection efficiency. The cells cotransfected with a combination of pACT and pBIND plasmid DNAs, and pID and pMYoD plasmid DNAs, served as negative and positive assay controls, respectively (Promega).

We also included plasmid DNA constructs encoding alanine mutations for D-2→A and NYTXXXRG-12–19→AAAXXXAA amino acids of SPA4 peptide (Mutagenex). The binding of SPA4 peptide and mutants to TLR4 was examined using the mammalian two-hybrid assay as described above. The restriction enzyme digestion and sequencing analyses confirmed the DNA sequences of the plasmid DNA constructs.

Radioligand-receptor binding assay.—The HYNIC-conjugated SPA4 peptide was labeled with [^{99m}Tc] radionuclide at the Research Imaging Facility, College of Pharmacy, OUHSC, Oklahoma City, OK. Briefly, an HYNIC-SPA4 peptide (30 μl of 2 mg/ml) was mixed with 200 μl of tricine (100 mg/ml aqueous solution), 40 μl of freshly prepared aqueous $SnCl_2.H_2O$ solution (10 mg/ml), and 200 μl of [^{99m}Tc]O_4 solution (10 mCi). The mixture was incubated for 30 min at room temperature, and the radiolabeled HYNIC-SPA4 peptide ([^{99m}Tc]-HYNIC-SPA4 peptide) was purified by gradient HPLC. We selected [^{99m}Tc] as a tracer radionuclide because of its relatively short half-life (6 h) and emission of a gamma ray of 140 keV, which could be used to assess biodistribution and half-life by imaging.

The pBIND-TLR4– or pBIND–vector plasmid DNA–transfected cells (as described above) were incubated with 25 μM of [^{99m}Tc]-HYNIC-SPA4 peptide per well for 30 min at 37°C in

Opti-MEM medium. The cells were washed twice with Opti-MEM medium and lysed with a buffer containing protease inhibitors (1 mM EDTA, 1.1 μM leupeptin, 1 μM pepstatin, and 0.2 mM phenylmethyl sulfonyl fluoride) and detergents (0.1% SDS and 1% Igepal CA630). The radioactivity was measured in a gamma well counter (Cobra II auto gamma counter; PerkinElmer, Waltham, MA). All radioactivity counts were decay corrected for [^{99m}Tc] decay (half-life 6 h). The counts were normalized with protein concentration, determined by the bicinchoninic acid assay (Pierce Biotechnology, Rockford, IL). Percentage of binding was calculated relative to that in the cells transfected with pBIND–vector plasmid DNA.

SPA4 peptide treatment

The JAWS II dendritic cells were seeded in α-modified MEM at a density of 1×10^6 cells per well. After incubation overnight, the cells were challenged with 100 ng/ml highly purified, low-protein, *Escherichia coli* O111:B4–derived LPS (L group; Calbiochem Research Biochemicals, San Diego, CA). The cells were then treated with 10 μM SPA4 peptide (L + S groups) or equivalent volume of vehicle to L group after 1, 3, or 4 h of LPS challenge or simultaneously. The cell-free supernatants and cells were harvested after 5 h of LPS challenge or at 15, 30, 45, 60, 90, and 120 min when cotreated simultaneously. The cell-free supernatants were obtained by centrifuging the culture medium at $120 \times g$ for 10 min and were stored at −80°C for analysis of cytokines and chemokines. Total cellular RNA was extracted using a commercially available kit (QIAGEN, Germantown, MD) and stored at −80°C for further analysis.

Experiments were also performed with synthetic alanine mutants of SPA4 peptide: D-2→A and NYTXXXRG-12–19→AAAXXXAA (GenScript). The JAWS II dendritic cells (1×10^6 cells) and primary mouse alveolar macrophages (0.5×10^6) were challenged with 100 ng/ml *E. coli* O111:B4 LPS and treated with 10 μM SPA4 peptide or alanine mutants 1 h after LPS challenge. An equivalent volume of diluent or solvent served as vehicle. The cell-free supernatants and cell lysates were collected at 5 h and stored at −80°C for further analysis.

In separate experiments, the cells were transfected with plasmid DNA encoding mouse wild-type or dominant-negative (P→H mutation) TLR4 (provided by Dr. L. Hajjar, University of Washington) in combination with NF-κB reporter plasmid DNA using TransIT-TKO transfection reagent (Mirus Bio, Madison, WI), as described earlier (17, 18). Transfected cells were challenged with 100 ng/ml LPS. The cells were treated with 10 μM SPA4 peptide (L + S group) after 4 h of LPS challenge. At 5 h of incubation, the luminescence readings for the NF-κB activity were normalized with total cellular protein, as described earlier (17, 18). Vehicle-treated cells served as controls.

RNA sequencing analysis

RNA sequencing (RNAseq) libraries were constructed using the Illumina TruSeq RNA LT v2 kit. The library construction was done using total RNA (500 ng to 1 μg). RNA quality for each preparation was analyzed on an Agilent Bioanalyzer 2100 prior to construction of the library using the nano RNA chips. Each library was indexed during library construction for sequencing on the Illumina MiSeq platform. Samples were normalized and sequenced in batches of two or three libraries per 2×150 bp paired-end sequencing run on the

Illumina MiSeq. On average, 46 million reads (seven-gigabyte size) of sequencing data were collected per run. Read counts, fragment counting statistics, strand specificity, adapter read-through, distribution of biotypes, and transcript length coverage were reviewed prior to data analysis. The CLC Genomics Workbench version 20.0.4 (QIAGEN) was used for data analysis. Raw sequence reads were mapped to the *Mus musculus* genome for identification of genes. At least three technical and three biological replicates were included for each group. Differential expression analysis was performed among two groups or throughout all groups at the whole transcriptome level. Differentially expressed genes among groups were identified on the basis of at least 2-fold change (absolute value > 2) in expression and *p* value of   0.05. Heat maps, Venn diagrams, and principal component analyses were performed to further determine the differential gene expression. In addition, datasets (fold change and *p* values) of differentially expressed genes were uploaded onto the Ingenuity Pathway Analysis program (QIAGEN) and assessed for canonical pathways, disease, function and physiology, and networks.

Mouse model of ALI

Mice were weighed and anesthetized with isoflurane, followed by administration of ketamine and xylazine. Anesthetized mice were then intratracheally instilled with 5 μg of *E. coli* O111:B4 LPS per gram body weight. After 1 h of LPS challenge, mice were treated with 50 μg of SPA4 peptide via the intratracheal route or were left untreated. Mice were then euthanized and necropsied after 4 h of LPS challenge, and bronchoalveolar lavage fluid (BALF) samples were collected.

BALF collection

For BALF collection, the thoracic cavity was opened, and an angiocatheter was inserted in the trachea. The lavage was performed by injecting 1 ml of sterile PBS without calcium and magnesium (Life Technologies, Thermo Fisher Scientific). The BALFs were centrifuged at $350 \times g$ for 5 min at 4°C. Supernatants were stored at −80°C for further analysis.

Flow cytometry

The BALF cells were pooled from animals in the same group, washed with PBS, and suspended in PBS (1×10^6 cells/100 μl). The cells were then resuspended in staining buffer (PBS containing 1% heat-inactivated FBS and 0.09% sodium azide). The FcγR was blocked by incubating the cells with anti-CD16/CD32 (eBioscience, San Diego, CA) Ab for 15 min on ice. The cells were then stained with 1 μg each in different combinations of FITC-conjugated Abs specific for CD123 (clone 5B11) and Ly6G/Gr1 (clone RB6–8C5), PE-conjugated Abs specific for CD11c (clone HL3) and CD68 (clone FA-11), PerCP coupled to cyanine dye (PerCPCy5.5)–conjugated Abs specific for CD11b (clone M1/70) and CD103 (clone: 2E7), allophycocyanin-conjugated Abs specific for F4/80 (clone: BM8), and biotin-conjugated Ab specific for I-A/I-E (or IAIE; clone 2G9). The cells were kept unstained or stained with a combination of Abs. The Abs were obtained from BD Biosciences (San Jose, CA), eBioscience, or BioLegend (San Diego, CA). Cells were incubated with the respective Abs for 20–30 min on ice in the dark, washed thrice with staining buffer, and fixed with 0.5% freshly prepared paraformaldehyde in PBS. Cells stained with biotin-conjugated Ab were stained with streptavidin–allophycocyanin conjugate before fixation. The cells were

analyzed on a BD Accuri C6 flow cytometer (BD Biosciences) within 24 h of staining. The gating strategies are shown in Supplemental Fig. 1. Unstained and stained BALF cells harvested from unchallenged, untreated mice served as controls.

Levels of cytokines (TNF-α, IL-1β, IL-6, IL-10, IL-12p35, IL-12p40, and IL-12p70) and chemokines (MIP-2, MCP-1, and keratinocyte-derived chemokine) in BALF- and cell-free supernatants

The BALF- and cell-free supernatants were subjected to ELISA to analyze TNF-α and IL-6, as per the method published earlier (17, 18). Commercial ELISA kits were used to measure the levels of IL-1β, IL-10, IL-12p40, and IL-12p70 (BioLegend); IL-12p35 (MyBioSource, San Diego, CA); and MIP-2, MCP-1, and keratinocyte-derived chemokine (KC) (R&D Systems, Minneapolis, MN) were used as per the method described by the manufacturer.

Statistics

Statistical significance was analyzed using ANOVA, followed by Tukey post hoc analysis for multiple comparisons test (Graph-Pad Prism software, La Jolla, CA). Statistical significance was defined at a p value <0.05 or as otherwise indicated.

RESULTS

SPA4 peptide and mutant peptides

In our previously published report, the SPA4 peptide region was shown to be in close proximity to the extracellular TLR4–MD2 complex through D-2, N-12, Y-12, T-14, R-18, and G-19 amino acids (19). Bioinformatic analyses of amino acid sequences of SPA4 peptide and alanine mutants (D-2→A and NYTXXXRG-12–19→AAAXXXAA) indicated low Boman indices or protein–protein-binding potential for both of the mutants (2.68 and 1.58 kcal/mol) compared with the Boman index of SPA4 peptide (3.2 kcal/mol). The alanine mutants were predicted to have increased total hydrophobic ratios (20 and 40%) compared with 15% for SPA4 peptide (Fig. 1A). Other physicochemical parameters and helical wheel chart analysis results are described in Fig. 1. The CD spectra were obtained for peptide solutions in 75% methanol. As referenced in our previously published article, CD spectra of SPA4 peptide in 75% methanol resulted in increased secondary structure demonstrating structural plasticity of the peptide (19). Fig. 1C shows the CD spectra of mutants relative to SPA4 peptide under these conditions.

The UV-VIS absorption spectrum of SPA4 peptide in water showed two peaks at 200–220 nm due to the backbone peptide bonds (π→π* and n→π*) and a third peak at 260–285 nm due to F-3, W-16, Y-5, Y-13, and Y-17 amino acids with aromatic rings. A significant shift of UV-VIS spectrum was noted with NYTXXXRG-12–19→AAAXXXAA in water. The spectrum of D-2→A in water paralleled with that of SPA4 peptide (Fig. 1D).

In silico predictions of changes in SPA4 peptide structure with alanine mutations and the interfaces with extracellular TLR4–MD2 complex

Changes were noted in the electrostatic potential of SPA4 peptide after alanine mutations of the respective amino acids were simulated (Fig. 2A). In the SPA4 peptide–TLR4–MD2

complex, the SPA4 peptide docked at the interface of TLR4 (chains A and B) and MD2 (chain D). We assessed the amino acids of TLR4 and MD2 chains around 5 Å of SPA4 peptide. The SPA4 peptide interfaced with both chains of dimerized TLR4 (K388, G389, V411, T413, M414, S415, S416, K435, Q436, and E439 of TLR4 chain A and R264, N339, K341, S360, N361, K362, G363, G364, R382, N383, G384, L385, F408, and N409 of TLR4 chain B) and a single chain of MD2 (I32, S33, I46, I52, L54, S57, L61, I63, F76, L78, I80, R90, K91, E92, V93, I117, F119, S120, F121, K122, G123, I124, F126, C133, V135, L149, F151, V152, and I153 of MD2) around 5 Å. The D-2→A mutation led to the loss of interface with TLR4 (at R264 of TLR4 chain B) (Fig. 2Biv). The NYTXXXRG-12–19→AAAXXXAA mutation resulted into the break of interfaces with MD2 (chain D; Fig. 2Bvi) along with a >5 Å shift of I32, S33, K91, V152, and I153 of MD2 chain D and N339 of TLR4 chain B around the peptide.

We also rendered the SPA4 peptide and created alanine mutations within the SPA4 peptide–TLR4–MD2 complex. The contacts (D2-F3, R4-R4, R4-S6, Y5-S6, 2× Y5-T14, S6-D7, N12-V11, N12-Y13, and N12-N15; polar contacts; and other contacts), clashes (2× D2-N15, within van der Waals distance ration <0.89) and π–π interaction (F3-Y5) were noted between the respective amino acids of SPA4 peptide within the computationally docked model. When D-2→A mutation was included, fewer contacts (R4-R4, R4-S6, Y5-S6, 2× Y5-T14, S6-D7, N12-V11, N12-Y13, and N12-N15) and the π–π interaction between F3-Y5 were retained, but the clashes were lost. The alanine mutation of NYTXXXRG motif resulted in a reduced number of contacts (D2-F3, R4-R4, R4-S6, Y5-S6, and S6-D7); the π–π interaction (F3-Y5) and clashes (2× D2-N15) remained intact within the model (Fig. 2B, 2C).

Binding of SPA4 peptide and peptide mutants to cellular TLR4 by two-hybrid assay

We analyzed the binding of SPA4 peptide and peptide mutants to TLR4 using an established mammalian two-hybrid system in HEK293 cells (Fig. 3A). The plasmid DNA constructs and principle of the assay are identified within the figure. In this approach, two separate plasmid DNAs encoded SPA4 peptide or mutants and TLR4 proteins, respectively. These vectors also encoded virion protein (VP)16 activation and galactose-responsive transcription factor GAL4 DNA binding domains. The pG5Luc vector contains five GAL4 binding sites upstream of the firefly luciferase gene that acts as a reporter for the interaction between the SP-A or SPA4 with TLR4. The binding of SPA4 peptide to TLR4 was assigned 100 relative luminescence units (RLU). Percentage change in RLU was determined for peptide mutants compared with SPA4 peptide binding to TLR4. The mutations D-2→A and NYTXXXRG-12–19→AAAXXXAA displayed 81 and 74% binding to TLR4 compared with the 100% binding of SPA4 peptide (Fig. 3B). The synthetic peptides encoding alanine mutations for both the D-2 amino acid and NYTXXXRG-12–19 motif of SPA4 peptide did not suppress the LPS-induced secreted levels of TNF-α cytokine. In comparison, the SPA4 peptide suppressed the LPS-induced TNF-α cytokine response (Fig. 3C, 3D).

SPA4 peptide binds to cellular TLR4 and exerts anti-inflammatory activity

For the radioligand-receptor binding assay, a bifunctional chelator, HYNIC, was conjugated to the SPA4 peptide. The HYNIC conjugation was at the extreme N-terminal end of the

SPA4 peptide. In the presence of tricine, HYNIC stably chelates [^{99m}Tc] radionuclide. Fig. 4A displays the chemical structure of the [^{99m}Tc]-HYNIC-SPA4 peptide. The binding of HPLC-purified [^{99m}Tc]-HYNIC-SPA4 peptide to TLR4 was assessed in HEK293 cells transfected with pBIND-TLR4 or pBIND–vector plasmid DNA. Upon decay correction and normalization of data for protein concentration, the radioactive counts associated with the cell fraction were compared. We found that [^{99m}Tc]-HYNIC-SPA4 peptide's association with pBIND-TLR4–transfected HEK293 cells was higher than its association with nontransfected or vector plasmid DNA–transfected HEK293 cells (Fig. 4C). When this radioligand-receptor interaction assay was performed in the presence of excess cold (unlabeled) SPA4 peptide, the radioactivity associated with the cell fraction was substantially reduced. The presence of excess cold SPA4 peptide had no influence on the cell-associated radioactive counts in nontransfected or vector plasmid DNA–transfected HEK293 cells (Fig. 4C). Furthermore, our results demonstrated that the SPA4 peptide treatment reduced the NF-κB activity of dendritic cells overexpressing TLR4 but did not change the NF-κB activity further in cells expressing dominant-negative TLR4 (Fig. 4D).

These results suggest the specificity of SPA4 peptide activity through its binding to TLR4.

SPA4 peptide does not affect the cell viability or size

The MTT assay results revealed that the SPA4 peptide did not affect the viability or metabolic activity of mouse JAWS II dendritic cells at the concentrations of 10 and 75 μM (Supplemental Fig. 2A). Trypan blue staining results also demonstrated that the SPA4 peptide treatment did not affect the viability or diameter of human HEK293 cells (Supplemental Fig. 2B–D).

Differential gene expression analysis in SPA4 peptide-treated cells

The dendritic cells were treated with SPA4 peptide after 4 h (L + S 4 h, exposed to the peptide for 1 h), 3 h (L + S 3 h, exposed to the peptide for 2 h), and 1 h (L + S 1 h, exposed to the peptide for 4 h) of LPS challenge.

The RNA samples with acceptable RNA integrity number (average 9.89) and 28s/18s rRNA ratios (average 1.94) were included. RNAseq report indicated 11,989,094–28,149,752 read counts and 97% fragments mapped to the genes among samples. Using the criteria of observing at least 2-fold change at p 0.05, the SPA4 peptide treatment affected −122- to +46-fold change in only 50 genes (upregulated genes: Gm43079, Cd247, Gm14416, Ccdc189, Gm26965, Gm15787, Zfp273, Hist2h2aa2, Psme2b, Zfp442, Calml4, 1700034H15Rik, 0610040B10Rik, Gm20517, Gm45713, Gm26888, Gm15429, A730015C16Rik, Gm9958, Gm15491, Rpl37rt; downregulated genes: A230056P14Rik, Nedd4l, Olfr934, Slc45a3, 4930524J08Rik, Glcci1, Gm26668, Reps2, Ccr5, Gm1980, Lif, 1810021B22Rik, Nr1i3, Aloxe3, Pla2g4b, Synpo2, Pdzd9, Osbp2, Gm26882, A830010M20Rik, Actg2, Adam18, Gm7889, 1700020D05Rik, Gm20388, Gm2260, Gm26508, Gm10275, Gm5601). The LPS challenge (L) induced −43- to +286-fold change in 1004 genes (Fig. 5). There were only 12 genes common in SPA4 peptide treatment (50 genes) and L groups (1004 genes) as compared with vehicle treatment (Fig. 5). After treatment with SPA4 peptide (L + S 1, 3, and 4 h), the changes were observed in expression

of 64–78 genes as compared with the L group (Fig. 5). We extended the differential gene expression analysis across all groups (vehicle treatment, SPA4 peptide treatment, L, L + S 1 h, L + S 3 h, and L+ S 4 h). The principal component analysis (PCA) demonstrated the clustering of the transcriptome in different groups. Differentially expressed genes in L group versus vehicle-treated group (1004 genes), L + S 1 h versus L group (64 genes), L + S 3 h versus L group (78 genes), and L + S 4 h versus L group (78 genes) are described in Supplemental Tables I and II.

We further compared and identified the upregulation and downregulation of common differentially expressed genes in comparative L versus vehicle-treated group (Supplemental Table I) and L + S groups versus L group (Supplemental Table II). The SPA4 peptide treatment reversed the expression of LPS-mediated upregulation of (noncoding RNA, histone cluster 2, putative TNF-resistance related protein, H6 homeobox 3, meiosis regulator and mRNA stability factor 1, B cell CLL/lymphoma 6 member B, chemokine [C-X-C motif] ligand 10, and IFN-induced protein with tetratricopeptide repeats 1) genes and LPS-mediated downregulation of (ER membrane protein complex subunit 1, X-linked Kx blood group related 5, TNF receptor superfamily member 14, opioid binding protein/cell adhesion molecule like, TNF superfamily member 13, KN-motif and ankyrin repeat domain 3, complement component 8 γ polypeptide, H3 clustered histone 8, stearoyl-CoA desaturase 4, protein phosphatase 1 regulatory inhibitor subunit 1A, tubulin α 1B, pseudogene, claudin 11, family with sequence similarity 171 member A2, growth differentiation factor 9, cation channel sperm associated auxiliary subunit γ 1, sedoheptulokinase, ArfGAP with SH3 domain ankyrin repeat and PH domain 2, TLR8, regulator of G-protein signaling 18, and *N*-acetylneuraminic acid phosphatase) genes (Fig. 5K).

Pathway analysis of differentially expressed genes

The SPA4 peptide treatment alone affected 50 genes and four network pathways: organ morphology, organismal development, organismal injury, and abnormalities; inflammatory disease, inflammatory response, organismal injury, and abnormalities; nervous system development and function, cancer, organismal injury, and abnormalities; and amino acid metabolism, small molecule biochemistry, and vitamin and mineral metabolism were identified compared with vehicle control. Pathway analysis of 1004 differentially expressed genes in the L group versus vehicle-treated group revealed top 25 networks of pathways mainly related to cell cycle, cell morphology, cellular assembly and organization, DNA replication, recombination, and repair, cardiovascular disease, cellular development, organismal injury and abnormalities, cell death and survival, cancer, hematological disease, cellular movement, hematological systems development and function, immune cell trafficking, antimicrobial response, infectious diseases, inflammatory response, cell-to-cell signaling and interaction, molecular transport, posttranslational modification, protein trafficking, endocrine system development and function, metabolic disease, tissue morphology, embryonic development, organ development, organ morphology, connective tissue disorders, inflammatory disease, tissue development, digestive system development and function, gastrointestinal disease, hepatic system development and function, humoral immune response, protein synthesis, gastrointestinal disease, developmental disorder, organismal development, cell signaling, lipid metabolism, small molecule biochemistry,

connective tissue development and function, and hereditary disorder. Three to six pathway networks were identified with differentially expressed genes in the L + S groups compared with the L group. In the L+ S 1 h group, the pathway networks involved cell-to-cell signaling and interaction, hematological system development and function, and inflammatory response; cancer, organismal injury and abnormalities, and reproductive system disease; cellular movement, connective tissue development and function, and nervous system development and function; cell death and survival, cell morphology, and cellular function and maintenance; and cardiac dilation, cardiac enlargement, and cardiovascular disease. The pathway analysis revealed effects on six networks (antimicrobial response, cell morphology, and nervous system development and function; amino acid metabolism, drug metabolism, and endocrine system development and function; cancer, cell morphology, and cellular development; DNA replication, recombination, and repair, hematological system development and function, and hematopoiesis; gene expression, nucleic acid metabolism, and small molecule biochemistry; and cell-to-cell signaling and interaction, cellular assembly and organization, and nervous system development and function) in the L +S 3 h group. Three networks of pathways related to lipid metabolism, molecular transport, and small molecule biochemistry; cellular development, cellular growth and proliferation, and embryonic development; and lipid metabolism, molecular transport, and small molecule biochemistry were affected by changes in gene expression in the L + S 4 h group as compared with the L group.

SPA4 peptide suppresses LPS-stimulated secretion of cytokines and chemokines

Our results demonstrated significant suppression of LPS-induced TNF-α, IL-1β, and KC levels after treatment with SPA4 peptide at all time points. However, the LPS-induced IL-6, IL-12p40, IL-12p70, MIP-2, and MCP-1 levels were significantly reduced after the cells were treated with SPA4 peptide for 1, 2, or 4 h (1 and 2 h [IL-6, MIP-2, and MCP-1], 1 and 4 h [IL-12p40], and 1 h [IL-12p70]; Fig. 6). The levels of IL-10 and IL-12p35 were not significantly altered in L + S groups. There was no significant difference in the IL-12p35/p70 and IL-12p40/p70 ratios between the L and L + S groups (Fig. 6).

The cotreatment with SPA4 peptide reduced the LPS-stimulated secretion of TNF-α, IL-1β, IL-6, KC, and MIP-2 after 45 min or 1 h. However, there was no significant change in the secreted levels of IL-10, IL-12p35, IL-12p40, IL-12p70, and MCP-1, or in the ratios of IL-12p35/p70 and IL-12p40/p70, any time during the 2-h study period (Fig. 7).

SPA4 peptide affects the cell immunophenotype and suppresses the cytokines and chemokines in BALFs

We focused on identifying the changes in neutrophil (CD11b and Gr1), monocyte, and macrophage (MHC class II [MHC II] or IAIE, CD11b, CD11c, CD14, CD68, and F4/80), and dendritic cell (MHC II or IAIE, CD11c, CD103, and CD123) populations in BALFs from unchallenged and untreated, LPS-challenged (left untreated), and LPS-challenged and SPA4 peptide–treated mice. The gating strategies are identified in Supplemental Fig. 1. As expected, the intratracheal challenge with LPS stimulated the percentages of $CD11b^{hi}Gr1^{hi}$ neutrophils, $Gr1^{+}CD11b^{med}$, and $Gr1^{+}CD11b^{hi}$ cell populations (gated based on the forward and side scatter and staining for CD11b and Gr1; Fig. 8A)

and CD11b⁺CD11c⁻, CD11b⁺CD11c⁺IAIE⁻CD14⁻, CD11b⁺CD11c⁻ IAIE^{lo}CD14^{lo-med}, CD11b⁻CD11c⁺IAIE^{hi}CD14^{lo-med} (gated based on the forward and side scatter, and staining for CD11b and CD11c and IAIE and CD14; Fig. 8B), CD11b⁺CD68^{lo}F4/80^{lo-med} (gated based on the forward and side scatter and staining for CD11b and CD68 and F4/80; Fig. 8C), and CD11b⁺CD14⁻(gated based on the forward and side scatter and staining for CD11b and CD14; Fig. 8D) macrophage populations in BALF specimens. The percentages of CD11b⁻CD11c⁻IAIE^{hi}CD14^{lo-med} (gated based on the forward and side scatter and staining for CD11b and CD11c and IAIE and CD14; Fig. 8B) and IAIE⁺CD11c^{hi}CD103^{hi}CD123^{hi} cell populations (gated based on the forward and side scatter and staining for IAIE, CD11c, and CD103 and CD123; Fig. 8E) decreased or only slightly altered. The levels of cytokines (TNF-α, IL-1β, and IL-6) and chemokines (MCP-1, MIP2, and KC) in the BALF supernatants harvested from LPS-challenged and SPA4 peptide–treated mice were significantly reduced compared with levels in LPS-challenged mice (Fig. 8G).

DISCUSSION

This report presents our findings on the mechanism of action of SPA4 peptide through its binding to TLR4. Earlier, we solved the structure of SPA4 peptide and identified the similarities with the homologous region within the neck–C-terminal–SP-A (PDB: 1R13) and computationally docked model of neck–C-terminal–SP-A in complex with extracellular–TLR4–MD2 (PDB: 3FXI) (15, 19, 28, 29). In the current study, we investigated the structure-activity relationship of SPA4 peptide at the subunit level using alanine mutants of D-2 amino acid and NYTXXXRG-12–19 motif, delineated the specificity of binding and activity of SPA4 peptide through TLR4, assessed the changes in gene expression profile and cytokine and chemokine response in a cell system, and determined the immune cell influx and cytokines and chemokines in BALFs from mice challenged with LPS and treated with SPA4 peptide.

The bioinformatic analyses predicted the structural conformations and physicochemical properties of SPA4 peptide and alanine mutations for the respective amino acids (Fig. 1). Notably, the protein-binding potential or Boman index, hydrophobicity, and electrostatic potential were altered with alanine mutations of D-2 amino acid and the NYTXXXRG-12–19 motif of SPA4 peptide (Figs. 1, 2). The CD and UV-VIS spectra indicated changes in structural conformation with alanine mutations (Fig. 1C, 1D). We next docked the top-ranked NMR structure of SPA4 peptide onto the extracellular TLR4–MD2 (PDB: 3FXI) and identified the clashes, contacts, and interfaces among atoms and residues around 5 Å of SPA4 peptide or mutants. The SPA4 peptide docked at the interface of TLR4 and MD2. Interestingly, the lipid A structure of LPS also interacts at a similar location (identified as TLR4* and MD-2* in Ref. 28). The D-2→A mutation caused the loss of some of the intrachain contacts, intrachain clashes originating from D-2, and interface with TLR4 chain B (at R264). The NYTXXXRG-12–19→AAAXXXAA also resulted in the loss of intrachain contacts, interfaced with MD2 at two different places, and >5 Å distance with N339 of TLR4 chain B (Fig. 2B, 2C). We next determined the binding of SPA4 peptide and alanine mutants to cellular TLR4 using a two-hybrid assay. Our results indicated loss of binding with both mutants. However, it was more pronounced with NYTXXXRG-12–

19→AAAXXXAA mutation (Fig. 3B). These results validate the intercalation of SPA4 peptide at the sites of LPS interfacing with TLR4 and MD2.

Treatment with the D-2→A and NYTXXXRG-12–19→AAAXXXAA mutations did not suppress the LPS-induced TNF-α in cell-free supernatants. As expected, the SPA4 peptide suppressed the LPS-induced cytokine response (Fig. 3C, 3D). We further used a complementary assay to determine the binding of [^{99m}Tc]-HYNIC-SPA4 peptide to cellular TLR4. The HYNIC linker was added to the peptide at an extreme N-terminal end of SPA4 peptide (Fig 4A). An increased level of [^{99m}Tc]-HYNIC-SPA4 peptide–associated radioactivity was observed in the lysates of HEK293 cells transfected with TLR4. Competition with plain SPA4 peptide significantly reduced the radioactive counts (Fig. 4C). The SPA4 peptide did not further suppress the NF-κB activity in cells expressing dominant-negative TLR4 (Fig. 4D). These results suggest the specificity of binding and activity of SPA4 peptide through TLR4.

The SPA4 peptide treatment did not affect the size or viability of HEK293 and JAWS II cells, indicating that the cells remained viable and healthy during SPA4 peptide treatment (Supplemental Fig. 2). Heat map, Venn diagram, and PCA analyses demonstrated that the SPA4 peptide only moderately affected the transcriptome of dendritic cells under the studied experimental conditions. The transcription of some of the genes were reversed by SPA4 peptide treatment in the L + S groups versus L group compared with the L group versus vehicle-treated cells. These observations corroborated with pathway analysis results that demonstrated an effect on four to six networks of pathways by SPA4 peptide treatment in L + S groups.

The altered cytokine response was observed in the post-LPS (after LPS) challenge model (Fig. 6), but not in the pre-LPS (before LPS) challenge model in a dendritic cell system (15). When added simultaneously with LPS, the SPA4 peptide began to decrease the LPS-induced cytokine response only after 45 min to 1 h (Fig. 7). These observations suggest that the short-term anti-inflammatory effects of SPA4 peptide are orchestrated through its intercalation with the LPS–TLR4–MD2 complex and alteration in intracellular signaling at protein levels. The levels of IL-10 were unaffected. This finding substantiates that the SPA4 peptide does not induce anti-inflammatory cytokine (IL-10) for reducing lung inflammation, but it suppresses the levels of proinflammatory cytokines and chemokines (TNF-α, IL-1β, IL-6, MIP-2, MCP-1, and KC) via binding to TLR4 and altered intracellular signaling. The unchanged IL-12 levels indicate that the SPA4 peptide treatment likely does not affect Ag processing and presentation.

To understand the biological relevance of results from in vitro experiments, we included a mouse model of intratracheal *E. coli* LPS challenge that induces lung inflammation (30). Our previously published results demonstrated that the intratracheally administered SPA4 peptide on its own did not induce toxicity or inflammation but suppressed the LPS-induced lung inflammation, edema, and biochemical markers of tissue injury in mice (30). As expected, the changes in BALF cell populations (increase in CD11b^{hi}Gr1^{hi}, Gr1^{+}CD11b^{hi}, Gr1^{+}CD11b^{med}, CD11b^{+}CD11c^{-}, CD11b^{+}CD11c^{+}IAIE^{-}CD14^{-}, CD11b^{+}CD11c^{-}IAIE^{lo}CD14^{lo-med},

CD11b$^-$CD11c$^+$IAIE^{hi}CD 14^{lo-med}, CD11b$^+$CD68^{lo}F4/80^{lo-med}, and CD11b$^+$CD14$^-$ cell populations and a slight alteration in CD11b$^-$CD11c$^-$ IAIE^{hi}CD14^{lo-med} and IAIE$^+$CD11c^{hi}CD103^{hi}CD123^{hi} cell populations) were noted in LPS-challenged mice. The influx of some of the cell populations was reduced by treatment with SPA4 peptide. Nonetheless, the BALF fluid specimens from mice in LPS-challenged and SPA4 peptide–treated group demonstrated significantly low levels of cytokines and chemokines (Fig. 8G) compared with those in LPS-challenged group. The reduced levels of proinflammatory cytokines and chemokines and unchanged IL-10 or IL-12 levels in L + S groups of JAWS II dendritic cells (Figs. 6, 7) suggest that the SPA4 peptide alleviated the LPS-induced lung inflammation and damage through its anti-inflammatory activity. The SP-A and SP-A regions in the form of short proteins or peptides have only recently been pursued for their host defense function against infectious or inflammatory stimuli. An SP-A peptide (Tyr^{161}–Lys^{201}) has been demonstrated to protect lung epithelium from cytotoxicity of human β-defensin 3 (31) and attenuate accumulation of mast cells and eosinophils (32). In a separate study, a functional trimeric recombinant fragment of human SP-A lacking the N-terminal domain was found efficacious in neutralizing respiratory syncytial virus (33). Efforts have also been directed to identify the lipid binding sites on SP-A (34). Earlier, the SP-A fragment (aa 114–144) was shown to bind to lipid and increase surface activity and lung compliance in a premature rabbit model (35). We have focused on studying the biological relevance of SPA4 peptide (aa 196–215) derived from the C-terminal end of human SP-A. Together, the results presented in this report suggest a mechanistic role of D and NYTXXXRG amino acids of SPA4 peptide for its binding and anti-inflammatory activity through TLR4.

Supplementary Material

Refer to Web version on PubMed Central for supplementary material.

ACKNOWLEDGMENTS

Abbreviations used in this article:

ALI	acute lung injury
ARDS	acute respiratory distress syndrome
BALF	bronchoalveolar lavage fluid
CD	circular dichroism

HEK	human embryonic kidney epithelial
HYNIC	hydrazinonicotinamide
IAIE	I-A and I-E
KC	keratinocyte-derived chemokine
L	LPS-challenged cell
L + S	LPS-challenged and SPA4 peptide–treated cell
MD2	myeloid differentiation protein 2
MHC II	MHC class II
NMR	nuclear magnetic resonance
OUHSC	University of Oklahoma Health Sciences Center
PCA	principal component analysis
PDB	Protein Data Bank
RLU	relative luminescence unit
RNAseq	RNA sequencing
SP-A	surfactant protein-A
UV-VIS	UV-visible
VP	virion protein

REFERENCES

1. Han S, and Mallampalli RK. 2015. The acute respiratory distress syndrome: From mechanism to translation. J. Immunol. 194: 855–860. [PubMed: 25596299]

2. Matthay MA, and Zemans RL. 2011. The acute respiratory distress syndrome: pathogenesis and treatment. Annu. Rev. Pathol. 6: 147–163. [PubMed: 20936936]

3. Standiford TJ, and Ward PA. 2016. Therapeutic targeting of acute lung injury and acute respiratory distress syndrome. Transl. Res. 167: 183–191. [PubMed: 26003524]

4. Ruthman CA, and Festic E. 2015. Emerging therapies for the prevention of acute respiratory distress syndrome. Ther. Adv. Respir. Dis. 9: 173–187. [PubMed: 26002528]

5. Hodgson MJ, Bracker A, Yang C, Storey E, Jarvis BJ, Milton D, Lummus Z, Bernstein D, and Cole S. 2001. Hypersensitivity pneumonitis in a metal-working environment. Am. J. Ind. Med. 39: 616–628. [PubMed: 11385646]

6. Schwartz DA, Thorne PS, Yagla SJ, Burmeister LF, Olenchock SA, Watt JL, and Quinn TJ. 1995. The role of endotoxin in grain dust-induced lung disease. Am. J. Respir. Crit. Care Med. 152: 603–608. [PubMed: 7633714]

7. Reed CE, and Milton DK. 2001. Endotoxin-stimulated innate immunity: A contributing factor for asthma. J. Allergy Clin. Immunol. 108: 157–166. [PubMed: 11496229]

8. Michel O, Kips J, Duchateau J, Vertongen F, Robert L, Collet H, Pauwels R, and Sergysels R. 1996. Severity of asthma is related to endotoxin in house dust. Am. J. Respir. Crit. Care Med. 154: 1641–1646. [PubMed: 8970348]

9. Wu X, Kong Q, Xia Z, Zhan L, Duan W, and Song X. 2019. Penehyclidine hydrochloride alleviates lipopolysaccharide-induced acute lung injury in rats: potential role of caveolin-1 expression upregulation. Int. J. Mol. Med. 43: 2064–2074. [PubMed: 30864740]

10. Xu M, Wang C, Li N, Wang J, Zhang Y, and Deng X. 2019. Intraperitoneal injection of acetate protects mice against lipopolysaccharide (LPS)-induced acute lung injury through its anti-inflammatory and anti-oxidative ability. Med. Sci. Monit. 25: 2278–2288. [PubMed: 30921298]

11. Wu Y, Singer M, Thouron F, Alaoui-El-Azher M, and Touqui L. 2002. Effect of surfactant on pulmonary expression of type IIA PLA(2) in an animal model of acute lung injury. Am. J. Physiol. Lung Cell. Mol. Physiol. 282: L743–L750. [PubMed: 11880300]

12. Aeffner F, Bolon B, and Davis IC. 2015. Mouse models of acute respiratory distress syndrome: A review of analytical approaches, pathologic features, and common measurements. Toxicol. Pathol. 43: 1074–1092. [PubMed: 26296628]

13. Beutler B. 2000. Tlr4: central component of the sole mammalian LPS sensor. Curr. Opin. Immunol. 12: 20–26. [PubMed: 10679411]

14. Awasthi S, Madhusoodhanan R, and Wolf R. 2010. Surfactant protein-A and toll-like receptor-4 modulate immune functions of preterm baboon lung dendritic cell precursor cells. Cell. Immunol. 268: 87–96.

15. Awasthi S, Brown K, King C, Awasthi V, and Bondugula R. 2011. A toll-like receptor-4-interacting surfactant protein-A-derived peptide suppresses tumor necrosis factor-α release from mouse JAWS II dendritic cells. J. Pharmacol. Exp. Ther. 336: 672–681. [PubMed: 21159752]

16. Rakhesh M, Cate M, Vijay R, Shrikant A, and Shanjana A. 2012. A TLR4-interacting peptide inhibits lipopolysaccharide-stimulated inflammatory responses, migration and invasion of colon cancer SW480 cells. OncoImmunology 1: 1495–1506. [PubMed: 23264896]

17. Ramani V, Madhusoodhanan R, Kosanke S, and Awasthi S. 2013. A TLR4-interacting SPA4 peptide inhibits LPS-induced lung inflammation. Innate Immun. 19: 596–610. [PubMed: 23475791]

18. Ramani V, and Awasthi S. 2015. Toll-like receptor 4-interacting SPA4 peptide suppresses the NLRP3 inflammasome in response to LPS and ATP stimuli. J. Leukoc. Biol. 98: 1037–1048. [PubMed: 26254306]

19. Awasthi S, Anbanandam A, and Rodgers KK. 2015. Structure of a TLR4-interacting SPA4 peptide. RSC Advances 5: 27431–27438. [PubMed: 25870755]

20. Gautier R, Douguet D, Antonny B, and Drin G. 2008. HELIQUEST: a web server to screen sequences with specific alpha-helical properties. Bioinformatics 24: 2101–2102. [PubMed: 18662927]

21. Conchillo-Sole O, de Groot NS, Aviles FX, Vendrell J, Daura X, and Ventura S. 2007. AGGRESCAN: a server for the prediction and evaluation of "hot spots" of aggregation in polypeptides. BMC Bioinformatics 8: 65. [PubMed: 17324296]

22. Kozlowski LP 2016. IPC - isoelectric point calculator. Biol. Direct 11: 55. [PubMed: 27769290]

23. Wang G, Li X, and Wang Z. 2015. APD3: the antimicrobial peptide database as a tool for research and education. Nucleic Acids Res. 44: D1087–D1093. [PubMed: 26602694]

24. Gasteiger E, Hoogland C, Gattiker A, Duvaud S, Wilkins MR, Appel RD, and Bairoch A. 2005. Protein identification and analysis tools on the ExPASy server. In The Proteomics Protocols Handbook. Walker JM, ed. Springer Protocols Handbooks. Humana Press, Totowa, NJ p. 571–607.

25. Dolinsky TJ, Nielsen JE, McCammon JA, and Baker NA. 2004. PDB2PQR: an automated pipeline for the setup of Poisson-Boltzmann electrostatics calculations. Nucleic Acids Res. 32: W665–W667. [PubMed: 15215472]

26. Tovchigrechko A, and Vakser IA. 2006. GRAMM-X public web server for protein-protein docking. Nucleic Acids Res. 34: W310–W314. [PubMed: 16845016]

27. Mosmann T 1983. Rapid colorimetric assay for cellular growth andsurvival: application to proliferation and cytotoxicity assays. J. Immunol. Methods 65: 55–63. [PubMed: 6606682]

28. Park BS, Song DH, Kim HM, Choi BS, Lee H, and Lee JO. 2009. The structural basis of lipopolysaccharide recognition by the TLR4-MD-2 complex. Nature 458: 1191–1195. [PubMed: 19252480]

29. Head JF, Mealy TR, McCormack FX, and Seaton BA. 2003. Crystal structure of trimeric carbohydrate recognition and neck domains of surfactant protein A. J. Biol. Chem. 278: 43254–43260. [PubMed: 12913002]

30. Awasthi S, Rahman N, Rui B, Kumar G, Awasthi V, Breshears M,and Kosanke S. 2020. Lung and general health effects of Toll-like receptor-4 (TLR4)-interacting SPA4 peptide. BMC Pulm. Med. 20: 179. [PubMed: 32576172]

31. Saito A, Ariki S, Sohma H, Nishitani C, Inoue K, Ebata N, Takahashi M, Hasegawa Y, Kuronuma K, Takahashi H, and Kuroki Y. 2012. Pulmonary surfactant protein A protects lung epithelium from cytotoxicity of human β-defensin 3. J. Biol. Chem. 287: 15034–15043. [PubMed: 22418431]

32. Uehara Y, Takahashi M, Murata M, Saito A, Takamiya R, Hasegawa Y, Kuronuma K, Chiba H, Hashimoto J, Sawada N, et al. 2017. Surfactant protein A (SP-A) and SP-A-derived peptide attenuate chemotaxis of mast cells induced by human β-defensin 3. J. Biol.chem. Biophys. Res. Commun. 485: 107–112.

33. Watson A, Kronqvist N, Spalluto CM, Griffiths M, Staples KJ, Wilkinson T, Holmskov U, Sorensen GL, Rising A, Johansson J, et al. 2017. Novel expression of a functional trimeric fragment of human SP-A with efficacy in neutralisation of RSV. Immunobiology 222: 111–118. [PubMed: 27793398]

34. Goh BC, Wu H, Rynkiewicz MJ, Schulten K, Seaton BA, and McCormack FX. 2016. Elucidation of lipid binding sites on lung surfactant protein a using x-ray crystallography, mutagenesis, and molecular dynamics simulations. Biochemistry 55: 3692–3701. [PubMed: 27324153]

35. Walther FJ, David-Cu R, Leung C, Bruni R, Hernández-Juviel J, Gordon LM, and Waring AJ. 1996. A synthetic segment of surfactant protein A: structure, in vitro surface activity, and in vivo efficacy. Pediatr. Res. 39: 938–946. [PubMed: 8725252]
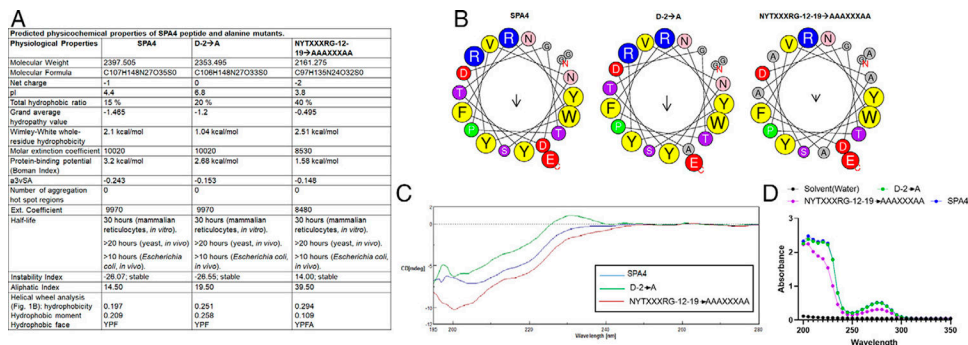
FIGURE 1. Structural, physicochemical, and functional attributes of SPA4 peptide.
Predictions about the physicochemical properties (isoelectric point, charge, hydrophobicity, Boman index, half-life, and stability) of SPA4 peptide and alanine mutants for D, N, Y, T, R, and G amino acids (**A**). Helical wheel diagram and analysis of polar, nonpolar, and hydrophobic faces of the peptide and alanine mutants (**B**). CD spectra of SPA4 peptide and alanine mutants diluted in 75% methanol. The CD spectroscopy was performed three times on separate occasions. An overlay of CD spectra is shown in (**C**). The UV-VIS spectrum (200–350-nm wavelength) of SPA4 peptide and alanine mutants is shown in (**D**). The CD and UV-VIS spectra were obtained in blinded fashion. Results are derived from three experiments performed on separate occasions
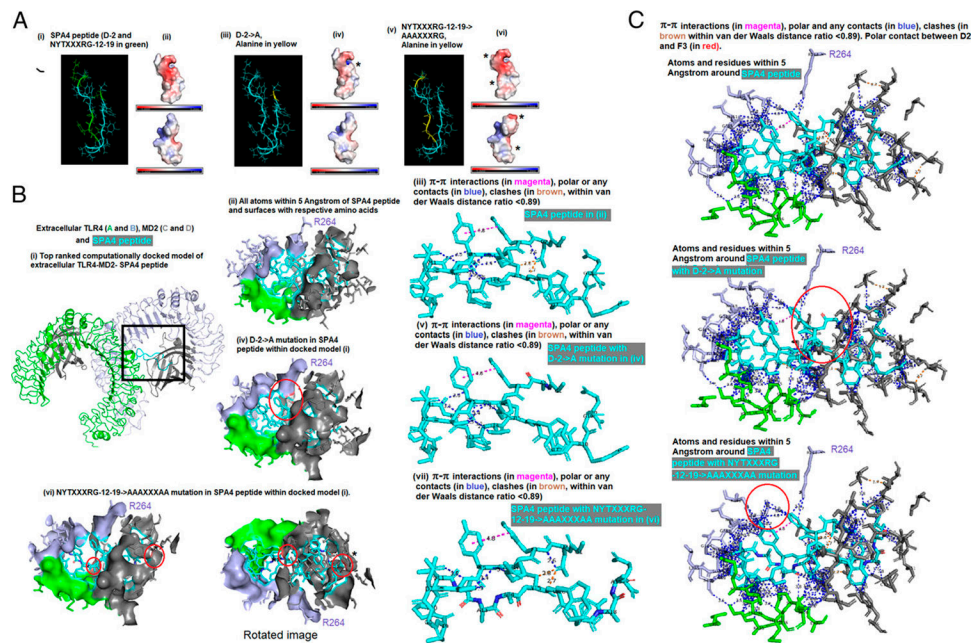
FIGURE 2. In silico analysis of the top-ranked NMR structure of SPA4 peptide and computationally docked structure of SPA4 peptide–extracellular TLR4–MD2 (PDB: 3FXI). The top-ranked solved NMR structure of SPA4 peptide was rendered for electrostatic potential. Respective amino acids were mutated to alanine within the NMR structure and electrostatic potential was assessed using the Adaptive Poisson-Boltzmann Solver plug-in within PyMOL (**Ai–Avi**). The SPA4 peptide structure was docked onto the extracellular TLR4–MD2 (PDB: 3FXI). The atoms and residues around 5 Å of SPA4 peptide, and surfaces between the SPA4 peptide, TLR4, (chains A and B) and MD2 (chain D) were identified (**Bi–iii**). The D-2 amino acid and NYTXXXRG-12–19 motif within the computationally docked model were mutated to alanine and peptide structure, and protein interfaces were studied for changes in contacts, clashes, and distances. Altered interfaces between SPA4 D-2→A mutant and TLR4 chain B, and SPA4 NYTXXXRG-12–19→AAAXXXAA mutant and MD2 chain D, are identified in (**Biv–vii**). The changes in interfaces and contacts were further identified at the amino acid level within the computationally docked model (**C**). The square, asterisk, and red circles are drawn to indicate the interfaces and orientation of the computationally docked model. The top-ranked solved structure of SPA4 peptide was published in Ref. 19
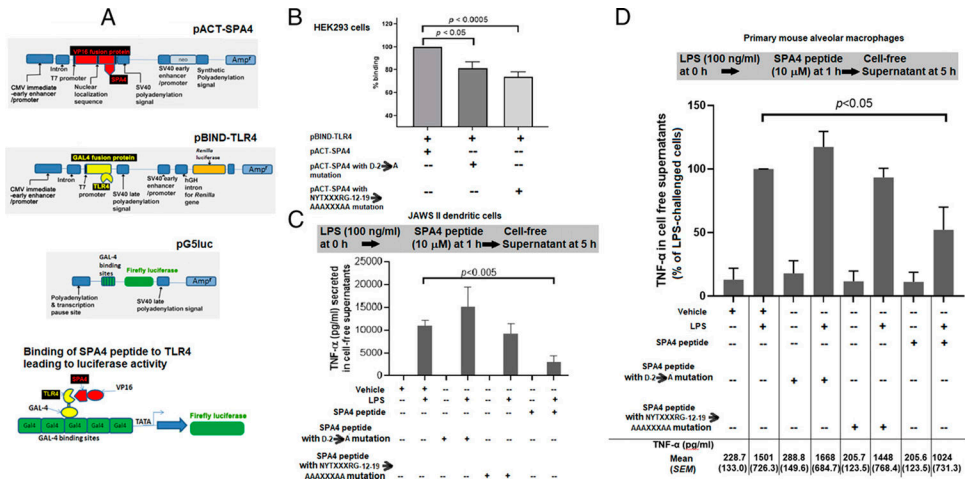
FIGURE 3. Binding of SPA4 peptide and alanine mutants to TLR4 and TNF-α cytokine response against LPS challenge at a cellular level.

Maps of plasmid DNA constructs encoding SPA4 (pSPA4) or D-2→A and NYTXXXRG-12–19→AAAXXXAA, TLR4 (pTLR4) cDNAs, and pG5Luc and the principle of the mammalian two-hybrid assay are shown in (**A**). In this assay, the HEK293 cells were cotransfected with pACT-SPA4 (or encoding alanine mutations), pBIND-TLR4, and pG5luc plasmid DNAs. The interaction between SPA4 with TLR4 leads to activation of firefly luciferase. Renilla luciferase allows for normalization of differences in transfection efficiency. The pACT and pBIND plasmid DNAs served as vector plasmid controls. RLU readings for SPA4 and TLR4 interaction in cells transfected with pACT-SPA4 and pBIND-TLR4 were set at 100. The bars represent mean + SEM of results obtained from 13 independent experiments performed separately in triplicate (**B**). The JAWS II dendritic cells were challenged with LPS at 0 h and treated with 10 μM SPA4 peptide or alanine mutants (D-2→A and NYTXXXRG-12–19→AAAXXXAA) 1 h post-LPS challenge. The cell-free supernatants were harvested at 5 h, and levels of TNF-α were measured by ELISA. The bars are mean + SEM (SE of measurement) values from four independent experiments performed on separate occasions (**C**). Similarly, primary mouse alveolar macrophages were challenged with LPS at 0 h and treated with 10 μM SPA4 peptide or alanine mutants (D-2→A and NYTXXXRG-12–19→AAAXXXAA) 1 h post-LPS challenge. An equivalent volume of diluent or solvent served as vehicle. The cell-free supernatants were harvested at 5 h, and levels of TNF-α were measured by ELISA. The results are shown as percentage of the TNF-α levels detected in LPS-challenged cells. The bars are mean + SEM values from five independent experiments performed on separate occasions. The mean (SEM) values of TNF-α (in picograms per milliliter) are also shown in (**D**). The assays were performed by three independent personnel, who were blinded for the mutations and peptide sequences. The p values were determined by ANOVA with Tukey post hoc analysis (B–D).
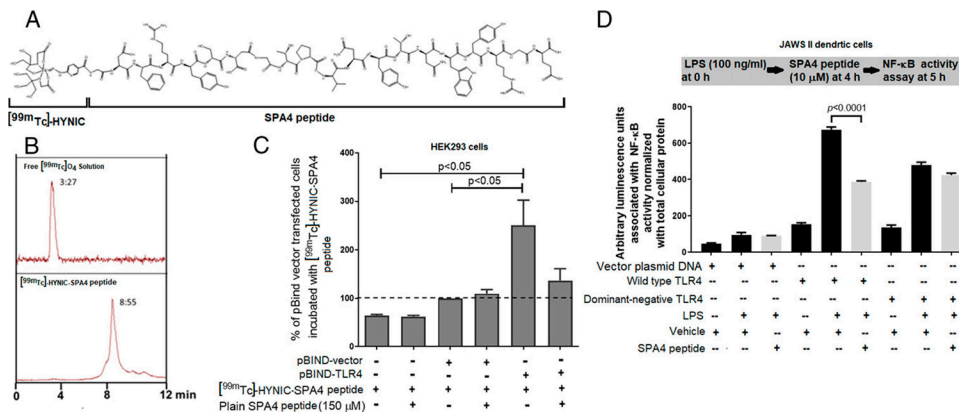
FIGURE 4. SPA4 peptide binding and activity through TLR4 at a cellular level by radioligand-receptor binding and NF-κB activity assays.

The HEK293 cells transfected with pBIND vector or pBIND-TLR4 plasmid DNA (Fig. 3) were used for a radioligand-receptor binding assay. Chemical structure of [^{99m}Tc]-HYNIC-SPA4 peptide (or Tracer) (**A**). The HPLC chromatograms depict the peak of free [^{99m}TcO$_4$] and [^{99m}Tc]-HYNIC-SPA4 peptide (**B**). Binding of [^{99m}Tc]-HYNIC-SPA4 peptide, with or without plain SPA4 peptide, to pBIND vector–transfected and pBIND-TLR4–transfected HEK293 cells. Competition with plain SPA4 peptide served as control. Bars represent mean + SEM of results from three experiments performed separately (**C**). The JAWS II dendritic cells were cotransfected with plasmid DNAs encoding mouse wild-type or dominant-negative TLR4 (P→H mutation) or vector and NF-κB reporter, challenged with LPS, and treated with SPA4 peptide. Arbitrary luminescence units associated with NF-κB activity were normalized with total cellular protein. Vehicle-treated cells served as control. Bars shown are mean + SEM of results in triplicate from one experiment representative of three experiments performed separately (**D**). The *p* values determined by ANOVA with Tukey post hoc analysis are shown within the figures (C and D).
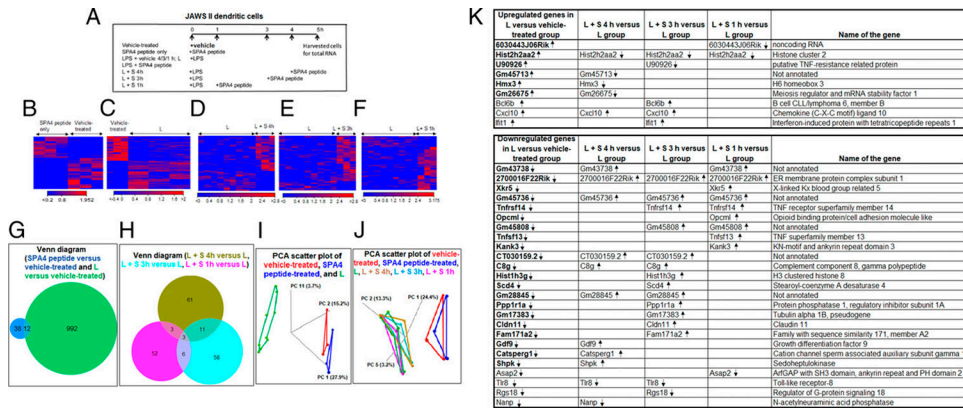
FIGURE 5. Heat maps, Venn diagrams, and PCA scatter plots demonstrating differential gene expression and clustering of RNAseq data from JAWS II dendritic cells (vehicle, SPA4 peptide only, L, and L + S treatments).

The time schedule for LPS challenge and vehicle or SPA4 peptide treatment is shown within the figure (**A**). All RNAseq data from cells challenged with LPS and treated with vehicle at different times (1, 3, and 4 h) were pooled into the L group. The cells were treated with SPA4 peptide after 4 h (denoted as L + S 4 h), 3 h (L + S 3 h), and 1 h (L + S 1 h) post-LPS challenge. All upregulated and downregulated genes were noted for at least 2-fold change (absolute value > 2) at p 0.05. Results are from three independent experiments performed separately on different occasions. Heat map analyses are shown for comparison of RNAseq data for SPA4 peptide alone versus vehicle-treated, L versus vehicle-treated, L + S 4 h versus L, L + S 3 h versus L, and L + S 1 h versus L (**B–F**). Venn diagrams demonstrate changes in expression between SPA4 peptide alone versus vehicle-treated (**G**), L versus vehicle-treated cells (G), and L + S 4 h versus L, L + S 3 h versus L, and L + S 1 h versus L study groups (**H**). PCA scatter plot shows the distribution and clustering of the data (**I** and **J**) from three or nine replicates from three separate experiments. Upregulation or downregulation of common differentially expressed genes in comparative groups of L versus vehicle-treated and L + S groups versus L group are shown in (**K**). All differentially expressed genes in comparative groups of L versus vehicle-treated and L + S groups versus L group are described in Supplemental Tables I and II.
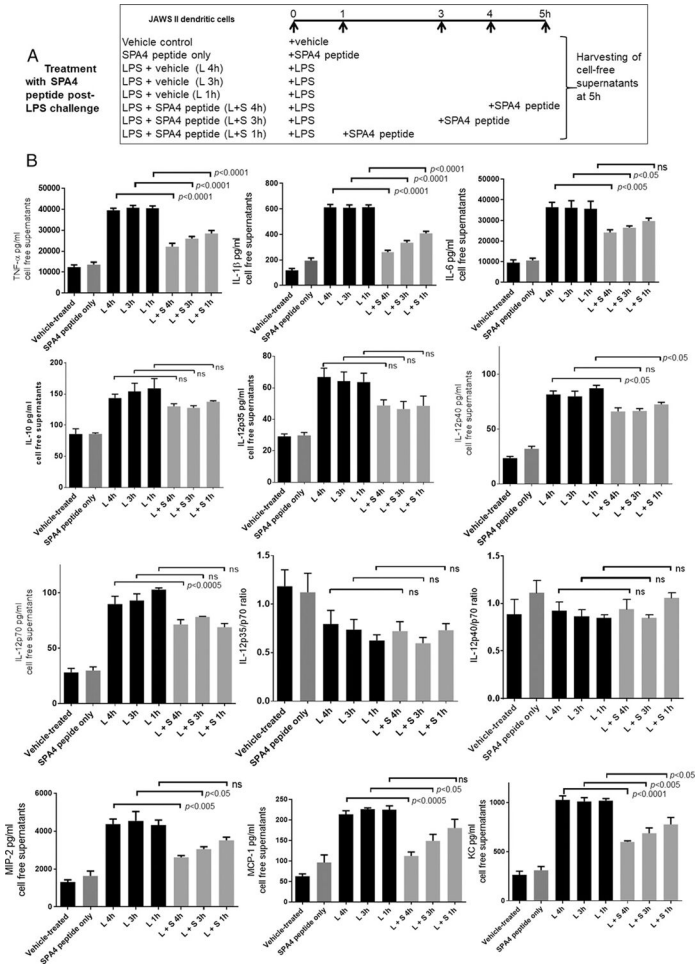
FIGURE 6. Levels of cytokines and chemokines in cell-free supernatants of JAWS II dendritic cells treated with SPA4 peptide post-LPS challenge.

The schedule of LPS challenge and SPA4 peptide treatment is shown in (**A**). The cytokines (TNF-α, IL-1β, IL-6, IL-10, IL-12p35, IL-12p40, and IL-12p70) and chemokines (MIP-2, MCP-1, and KC) were measured in cell-free supernatants harvested after 5 h. The *p* values determined by ANOVA with Tukey post hoc analysis are shown within the figure (**B**). ns, not significant.
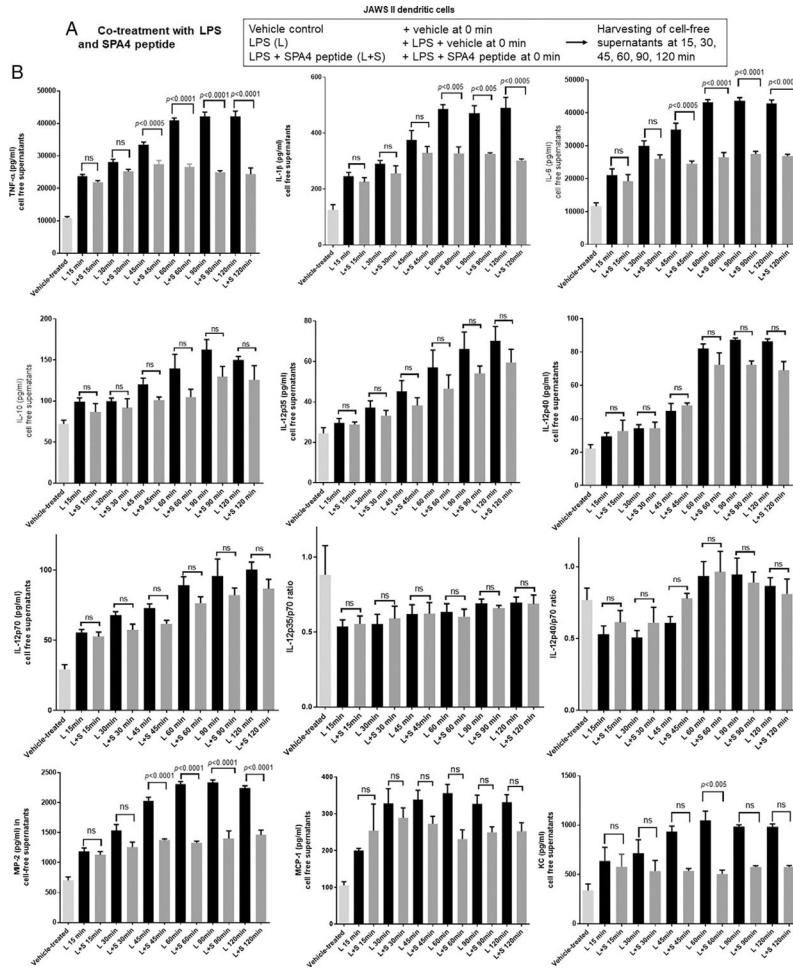
FIGURE 7. Levels of cytokines and chemokines in cell-free supernatants of cells treated with LPS and SPA4 peptide simultaneously.

The schedule of LPS challenge and SPA4 peptide treatment is shown in (**A**). The cytokines (TNF-α, IL-1β, IL-6, IL-10, IL-12p35, IL-12p40, and IL-2p70) and chemokines (MIP-2, MCP-1, and KC) were measured in cell-free supernatants collected from JAWSII dendritic cells (vehicle, L, and L + S treatments) after 15, 30, 45, 60, 90, and 120 min. The p values determined by ANOVA with Tukey post hoc analysis are shown within the figure (**B**). ns, not significant.

Mean (SEM) percentage of cell populations. Results are derived from seven mice per study group included in two experiments.

Analysis shown in	Cell populations	Unchallenged, Untreated	LPS-challenged	LPS-challenged, SPA4 peptide-treated
(A)	CD11b^hi^Gr1^hi^	0.4 (0.4)	4.2 (0.1)	1.2 (0.6)
	CD11b^hi^ Gr1^med-hi^	1.3 (1.2)	0.75 (0.45)	0.75 (0.45)
	Gr1+CD11b^hi^ (M1 gate)	9.05 (8.27)	54.81 (1.93)	29.77 (1.25)
	Gr1+CD11b^med^ (M2 gate)	9.63 (6.89)	22.55 (4.45)	31.83 (5.94)
(B)	CD11b+CD11c-	8.3 (3.0)	75.8 (3.8)	58.55 (6.75)
	CD11b+CD11c+IAIE-CD14-	37.2 (7.4)	67.35 (7.35)	49.05 (10.95)
	CD11b+CD11c-IAIE^hi^CD14^lo-med^	69.25 (9.25)	91.6 (0.7)	87.6 (1.2)
	CD11b-CD11c+IAIE^hi^CD14^lo-med^	21.55 (1.25)	26.9 (16.4)	24.9 (12.0)
	CD11b-CD11c-IAIE^hi^CD14^lo-med^	3.35 (3.15)	1.3 (0.7)	0.9 (0.4)
(C)	CD11b+CD68^hi^F4/80^lo-med^	17.55 (3.35)	62.2 (2.8)	46.1 (14)
(D)	CD11b+CD14-	0.75 (0.65)	6.65 (0.85)	1.5 (0.5)
(E)	IAIE+CD11c^hi^CD103^hi^CD123^hi^	17.5 (0.4)	18.10 (5.6)	14.2 (2.9)

FIGURE 8. Immune cell profile and levels of cytokines and chemokines in BALFs from mice challenged with LPS and treated with SPA4 peptide.

Mice were intratracheally challenged with LPS (5 µg/g body weight) at 0 h and intratracheally treated with SPA4 peptide (50 µg/mouse) at 1 h after LPS challenge. Unchallenged, untreated mice served as control. The BALFs were collected at 4 h after LPS challenge, and cells were harvested after centrifugation. The BALF cells were stained with mixtures of fluorochrome-conjugated, marker-specific Abs for respective immune cells. The immunostaining was determined by flow cytometry. Percentage of gated cells and different cell population types were identified. The gating was based on initial gate on forward and side scatter of cells and subsequently on staining for CD11b and Gr1 (**Ai** and **Aii**), CD11b and CD11c, and IAIE (or MHC II) and CD14 (**B**), CD11b, and CD68 and F4/80 (**C**), CD11b and CD14 (**D**), and IAIE, CD11c, and CD103 and CD123 (**E**) markers. The gating strategies are identified in Supplemental Fig. 1. The asterisk (*) indicates the phenotype of BALF cells in unchallenged and untreated control mice that are most altered in mice in LPS-challenged (left untreated, LPS group, central lane) and LPS-challenged, SPA4 peptide–treated (LPS + SPA4 peptide) groups. Percentages of cells are listed in (**F**). The picogram per milliliter levels of cytokines (TNF-α, IL-1β, and IL-6) and chemokines (MIP-2, MCP-1, and KC) detected in BALF supernatants are shown in (**G**). Results (mean + SEM) are from two experiments performed on different occasions (*n* = 6–9 mice per group). The *p* values determined by ANOVA with Tukey post hoc analysis are shown within the figures.